Journal of
Pharmaceutical and BioTech Industry

MDPI

Article

Multi-Level Drug Delivery System Integrated with Injectable Hydrogels and ZIF-8 for Sustained Release of Lidocaine

Lei Jiang [1,2,3], Fan Fan [1,2,3], Xuemei Wang [1], Shaukat Ali [4], Feng Zhou [1,2,3] and Jiantao Zhang [1,2,3,*]

[1] Laboratory of Advanced Theranostic Materials and Technology, Ningbo Institute of Materials Technology and Engineering, Chinese Academy of Sciences, Ningbo 315201, China; jianglei@nimte.ac.cn (L.J.)
[2] Ningbo Cixi Institute of Biomedical Engineering, Cixi 315300, China
[3] Zhejiang Key Laboratory of Biopharmaceutical Contact Materials, Ningbo Institute of Materials Technology and Engineering, Chinese Academy of Sciences, Ningbo 315201, China
[4] Scientific Affairs & Technical Marketing, Ascendia Pharma, Inc., North Brunswick, NJ 08902, USA
* Correspondence: zhangjiantao@nimte.ac.cn

Abstract: Lidocaine plays a significant role in postoperative analgesia by effectively reducing pain. However, due to its short half-life, it is challenging for lidocaine to achieve the desired duration of analgesia in clinical settings. Drug delivery systems can regulate the release rate over time, making them one of the most effective strategies for achieving sustained release. In this work, a multi-level drug delivery system was designed using hyaluronic acid-modified zeolitic imidazolate framework-8 (HA/ZIF-8) nanoparticles and injectable hydrogels composed of modified natural polymers. Lidocaine was incorporating into the modified ZIF-8 and uniformly dispersed within the hydrogel network. The dynamic light scattering (DLS) and Fourier transform infrared spectrometer (FTIR) results indicate the successful loading of lidocaine into ZIF-8, while the X-ray diffractometer (XRD) results confirm that the loading of lidocaine did not disrupt the crystal structure of ZIF-8. The coating of hyaluronic acid on ZIF-8 enhanced cell biocompatibility, with cell viability increasing by 89% at the same concentration. This multi-level drug delivery system can be injected through a 27-guage needle. In vitro release studies demonstrated a sustained release of lidocaine for more than 4 days and kinetic simulations aligned with the Bshakar model, indicating its potential for use in long-acting analgesic preparations.

Keywords: multi-level; drug delivery system; ZIF-8; injectable hydrogels; sustained release

Academic Editor: Vivek Gupta

Received: 20 December 2024
Revised: 1 February 2025
Accepted: 10 February 2025
Published: 14 February 2025

Citation: Jiang, L.; Fan, F.; Wang, X.; Ali, S.; Zhou, F.; Zhang, J. Multi-Level Drug Delivery System Integrated with Injectable Hydrogels and ZIF-8 for Sustained Release of Lidocaine. *J. Pharm. BioTech Ind.* **2025**, *2*, 3. https://doi.org/10.3390/jpbi2010003

1. Introduction

Postoperative pain is a common concern among patients who have undergone invasive surgical procedures. Typically manifesting within 72 h of surgery, this discomfort affects over half of all patients [1]. Effectively managing postoperative pain remains a significant hurdle in contemporary medical practice. Inadequate control of postoperative pain not only significantly compromises patients' quality of life and functional recovery but also heightens the likelihood of developing postoperative complications and prolongs their hospital stay [2]. Therefore, developing an effective strategy managing postoperative pain is crucial for facilitating a faster and smoother recovery process for patients.

Currently, opioids, non-steroidal anti-inflammatory drugs, and analgesic pumps are the standard methods used in clinical settings to manage postoperative pain [3,4]. Nevertheless, these approaches possess certain drawbacks. For instance, opioids may trigger severe side effects like nausea, vomiting, and respiratory depression during administration [5]. Analgesic pumps, on the other hand, require costly equipment and necessitate continuous

monitoring, while long-term catheter use is often associated with catheter displacement and other complications.

Recently, local anesthetics, such as lidocaine, bupivacaine, and ropivacaine, have become increasingly popular in postoperative pain management [6–8]. These anesthetics exhibit a pronounced analgesic effect with minimal complications by blocking the influx of sodium ions, which induces peripheral nerve blockade and results in local anesthesia. However, their clinical application in postoperative analgesia is limited due to their low molecular weight, short half-life, and potential cardiac and neurotoxic effects when administered in large doses [9]. In addition, local anesthetics for post-operative analgesia are currently given by slow intravenous infusion, e.g., from a syringe pump, to manage the level in blood required for pain relief, but this can lead to adverse events, such as infection caused by prolonged catheter retention. Therefore, there is an urgent need to develop novel delivery systems that can sustainably release local anesthetics with small molecular weights by subcutaneous injection to avoid the occurrence of adverse events.

In recent decades, the unprecedented advantages of micro/nano particles have led to broad applications in the field of biomedicine [10,11]. By regulating the composition, size, shape, and surface engineering of micro/nano materials, researchers can tailor their drug release behaviors. Among these materials, metal–organic framework materials are extensively employed for encapsulating hydrophobic drugs due to their low toxicity, high drug loading capacity, and easy degradation within the human body [12]. Zeolitic imidazolate framework-8 (ZIF-8), composed of Zn ions and imidazolate ligands, is a class of metal–organic frameworks that possess a similar structure as the conventional aluminosilicate zeolite. This material exhibits an inherent porous structure, a high loading capacity, and pH-induced degradation, as well as exceptional thermal and chemical stability. ZIF-8 has been employed to load various substances, including dapsone [12], dimethylglyoxime [13], CYP450 [14], and dacarbazine [14], for the protection and sustained release of these drugs.

Nevertheless, after the injection of local anesthetics, the high mobility of individual micro/nano particles may result in low drug utilization and challenges in achieving the therapeutic window. Injectable hydrogel formulations with high viscosity have the advantage of prolonging drug retention time [15,16]. The multi-level drug delivery system combining micro/nano particles with injectable hydrogel formulations can effectively address these issues. For instance, Eric Farrell et al. loaded BMP-2 protein into recombinant collagen peptide microspheres/alginate hydrogel, and the results showed a sustained release of BMP-2 [17]. Morgan V. DiLeo et al. encapsulated cysteamine, a treatment for cystinosis, into poly(lactic-co-glycolic acid) (PLGA) microspheres and suspended them in PNIPAM-based (poly(N-isopropyl acrylamide)) hydrogel for use in eye drop formulations [18]. The quantification of cysteamine in the eyes and plasma using LC-MS revealed that the sustained-release formulation maintained drug concentrations comparable to a single drop of eye drops for up to 12 h, demonstrating significantly improved sustained-release effects. Such multi-level drug delivery systems are also suitable for the sustained release of local anesthetic drugs. Currently, some research teams have used PLGA microspheres to encapsulate the local anesthetic bupivacaine and incorporate the microspheres into a PLGA-PEG-PLGA temperature-sensitive gel, achieving a sustained-release effect for up to 3 days in vitro [19,20]. However, synthesizing this type of material involves complex steps and requires stringent control over the tightness of the experimental equipment and the water content of raw materials, which increases the difficulty of material preparation. Therefore, it is of great significance to develop a simple yet efficient micro/nano-injectable gel drug delivery system.

Herein, we report a multi-level local anesthetic delivery system combining injectable hydrogel with nanoparticles, which provides continuous analgesia through injection at

a local location. Local anesthetic drugs were encapsulated in inorganic nanomaterials and coated with hyaluronic acid. Modified natural polymeric materials were utilized to construct injectable hydrogels through Schiff base bonds. Inorganic nanoparticles were suspended in the injectable hydrogel to prolong the retention time. These inorganic nanoparticles were uniformly distributed in the hydrogel matrix and exhibited significant sustained-release effects, providing drug release for up to 4 days, which meets the clinical requirements for post-operative analgesia. The formulation combines the advantages of nanotechnology and hydrogel systems to achieve controlled and sustained release of the lidocaine at the injection site. The nanoparticles are engineered to encapsulate the analgesic agent, ensuring stability and enhancing bioavailability, while the gel matrix facilitates localized depot formation, allowing for gradual lidocaine diffusion into the surrounding tissues. This approach minimizes systemic exposure, reduces dosing frequency, and improves patient compliance by offering long-lasting pain relief. The formulation is optimized for biocompatibility, injectability, and tunable release kinetics, making it a promising candidate for the management of chronic pain conditions.

2. Materials and Methods

All chemical reagents were used as received in the experiment without any purification. 2-Methylimidazole, sodium periodate ($NaIO_4$), 2-morpholinoethanesulfonic acid (MES), N-hydroxysuccinimide (NHS), and adipic dihydrazide (ADH) were purchased from Shanghai Aladdin Biochemical Technology Co., Ltd. (Shanghai, China). Zinc nitrate hexahydrate, methanol, sodium alginate, hyaluronic acid (HA, 200–400 kDa), gelatin, 1-(3-Dimethylaminopropyl)-3-ethylcarbodiimide (EDC), 1-Hydroxybenzotriazole (HOBt), and lidocaine were purchased from Shanghai Macklin Biochemical Co., Ltd. (Shanghai, China). Water was obtained from a Milli-Q Water Purification System from Millipore (Bedford, MA, USA). The L929 mouse fibroblast cells were obtained from Dalian Meilun Biotechnology Co., Ltd. (Dalian, China). The Cell Counting Kit-8 (CCK-8) was acquired from Shanghai Beyotime Biotechnology Co., Ltd. (Shanghai, China).

All the other chemicals and reagents used in the study were of analytical grade.

Morphology and microstructure characterization was carried out on a field emission scanning electron microscope (Hitachi Regulus 8230, Tokyo, Japan). The sample was dipped on the conductive adhesive, followed by 100 s of gold spraying, and then placed in the SEM sample chamber, vacuumed, and photographed under the conditions of 10 kV of acceleration voltage. Based on the SEM images of the hydrogel, the pore size of the gel was statistically measured, the scale in the image was calibrated, and the pore size was read by Nanomeasure software. The X-ray diffraction patterns were recorded on a diffractometer (Bruker, D8 Advance, λ = 1.542 Å, 45 kV, 200 mA). The UV–vis absorption spectra were determined by a UV spectro-photometer (TU-1810DASPC, Puxi General Instrument Co., Ltd., Beijing, China). FT-IR spectra were collected on a spectro-photometer (Nicolet iS50, Thermo Scientific, Waltham, MA, USA) using KBr pellets. The particle sizes of the products were determined using the dynamic light scattering (DLS) technique (Litesizer 500, Anton Paar, Graz, Austria).

2.1. Synthesis of ZIF-8@L

According to the literature, ZIF-8 was prepared using the hydrothermal method [21]. Specifically, 1 g each of organic linker 2-methylimidazole and lidocaine was dissolved in 4 mL of methanol solution and stirred at room temperature to form a transparent solution by using a magnetic stirrer, named solution A. At the same time, 0.1 g of zinc nitrate hexahydrate was dissolved in 2.4 mL of methanol solution and stirred to form a transparent solution, named solution B. Subsequently, solution B was slowly added

dropwise to solution A while stirring at 800 rpm for 20 min to produce lidocaine-loaded ZIF-8 (defined as ZIF-8@L). Then, the resulting ZIF-8@L was collected by centrifugation at 10,000 rpm for 10 min and washed three times with methanol. The supernatant solution was measured using UV–vis absorption spectra to determine the loading capacity of the lidocaine. The unloaded ZIF-8 was synthesized using the same protocol without lidocaine.

2.2. Synthesis of HA/ZIF@L

HA-functionalized ZIF-8@L (referred to as HA/ZIF@L) was acquired as follows. Hyaluronic acid aqueous solution with a concentration of 0.1 wt% was prepared with the assistance of a magnetic stirring process. Then, the ZIF-8@L obtained from the aforementioned preparation was dispersed in water to achieve a dispersion concentration of 0.1 mg/mL. Subsequently, 1 mL of the ZIF-8@L dispersion was mixed with 9 mL of a hyaluronic acid aqueous solution. The mixture was stirred for 24 h at room temperature, followed by centrifugation to collect the product.

2.3. Preparation of Gel/HZ@L

2.3.1. Synthesis of OSA

Oxidized sodium alginate (OSA) was synthesized according to a previously reported study [22]. First, 1 g of sodium alginate was dissolved in 99 mL of deionized water to prepare a 1 wt% sodium alginate aqueous solution. Then, 1.08 g of sodium periodate was added to the above sodium alginate solution, and stirring was maintained for 5 h under a dark environment at room temperature. Subsequently, 2 mL of ethylene glycol was added to quench the reaction. The product was precipitated with excess ethanol. Then, the OSA was collected by filtration and dialyzed (MWCO = 8000~10,000 Da) for 2 days. Finally, pure OSA was obtained by freeze-drying.

2.3.2. Synthesis of HA-ADH

Hydrazide modified hyaluronic acid (HA-ADH) was synthesized according to a previously reported study [23]. First, 0.1 M of MES buffer solution was prepared by dissolving a certain amount of MES with ultrasonic treatment. Then, 1 g of hyaluronic acid was dissolved in the MES solution to obtain a 1 wt% HA solution. Then, 1.04 g of ADH, 0.056 g of EDC, and 0.024 g of HOBt were added to the above HA solution, which was magnetically stirred for 48 h. The product was precipitated with excess ethanol and purified by dialysis and lyophilization.

2.3.3. Synthesis of Gel/HZ@L

The multi-level local anesthetic delivery system, which combines injectable hydrogel with nanoparticles, was formed by the in situ gelation of solutions of OSA, HA-ADH, gelatin, and HA/ZIF@L. Specifically, OSA and HA-ADH were dissolved in deionized water at room temperature to obtained aqueous solutions with concentrations of 50 mg/mL and 25 mg/mL, respectively. Meanwhile, a certain amount of gelatin was dissolved in water at 50 °C to obtain a 5% aqueous solution. Different masses of HA-ZIF@L were dispersed in 300 μL of OSA solution, and then mixed with HA-ADH and gelatin solutions using a vortex mixer to obtain Gel/HZ@L. The volume of OSA dispersion, HA-ADH, and gelatin solution was 400 μL, 300 μL, and 300 μL, respectively. The hydrogel was named Gel/HZ@L_0, Gel/HZ@L_1, Gel/HZ@L_2, Gel/HZ@L_3, and Gel/HZ@L_4 based on the increasing concentration of HA/ZIF@L. The detailed composition of Gel/HZ@L is shown in Table S1 in the Supplementary Materials.

2.4. Rheological Analysis

The rheological characteristics of the hydrogel Gel/HZ@L_0, Gel/HZ@L_1, Gel/HZ@L_2, Gel/HZ@L_3, and Gel/HZ@L_4 were measured using a rheometer with a conical plate geometry (TA, Discovery HR-2). The storage modulus (G′) and loss modulus (G″) of five hydrogels were measured using the strain sweep mode at 1 Hz. The capacity of the hydrogels to recover from strain deformation was measured by subjecting them to oscillating strains of 1% and 2000% every 30 s repeatedly, at a frequency of 1 Hz. All rheology experiments were conducted at 25 °C. Finally, an experiment to test the viscosity of the Gel/HZ@L_3 hydrogel as it varied with the shear rate was conducted with a shear rate in the range of 0–200 1/s, maintaining the frequency at 1 Hz and strain at 1.0%.

2.5. In Vitro Release Study

ZIF-8 is an acid-sensitive material, and the drug release behavior under acidic conditions is very different from that under neutral conditions. Generally, the rate of drug release is faster in acidic conditions than in neutral conditions. Subcutaneous tissue is likely to reflect a higher pH environment. Therefore, the release at pH 7.4 may mimic the drug release after subcutaneous injection. To study the release of lidocaine in vitro, 25 mg HA-ZIF@L and 1 mL Gel/HZ@L_3 were added to a 15 mL centrifuge tube, respectively. Then, 10 mL PBS (pH 7.4 or pH 5.4) as the release medium was added to the centrifuge tube. Next, the tubes were mechanically shaken in an incubator at 37 °C at 100 rpm. The release medium was sampled at the predetermined time for analysis and replenished with an equivalent volume of fresh release medium. A UV–vis spectrophotometer was used to monitor the supernatant at a wavelength of 263 nm to analyze the released concentration of lidocaine in the supernatant. The lidocaine release under acidic conditions was also carried out in the same way, except that the release medium was replaced by PBS with a pH of 5.4. The content of lidocaine in the release medium was calculated by a standard curve, and the cumulative release rate of lidocaine was calculated according to the following formula.

$$Q_t = \frac{C_t \times V_0 + \sum_1^t (C_t \times V)}{W} \times 100 \quad (1)$$

where Q_t is the cumulative release rate (%) of the lidocaine at each sampling point, C_t is the concentration of lidocaine at each sampling point, V_0 is the volume of the release medium, V is the sampling volume, and W represents the loading of the lidocaine.

Investigating the kinetics models of lidocaine release will make it possible to generate more insights into what drives the release process and mechanisms. The release model was selected in accordance with the potential release mechanisms, including diffusion and ion exchange. Four types of kinetics models (zero-order, first-order, Higuchi, and Bhaskar), after modification, were employed to investigate the lidocaine release kinetics from the carriers. These are summarized below.

Zero-order model:

$$Q_t = kt \quad (2)$$

First-order model:

$$Q_t = 1 - e^{-kt} \quad (3)$$

Higuchi model:

$$Q_t = kt^{1/2} \quad (4)$$

Bhaskar model:

$$Q_t = 1 - e^{-k(t-a)^{0.65}} \quad (5)$$

where Q_t is the cumulative release rate (%) of the lidocaine at each sampling point, t is the time, and k represents the rate constant. The diffusional exponent n is dependent on the geometry of the device and the release mechanism.

2.6. Biocompatibility of the Hydrogel

This experiment was conducted to study the cell toxicity of materials (ZIF@L only, HA-ZIF@L, and Gel/HZ@L_3). L929 mouse fibroblast cells were cultured with DMEM complete medium (containing 10% FBS, 1% PS) in a 37 °C incubator containing 5% CO_2. L929 cells were collected and spread into 96-well plates at a density of 2×10^3 cells per well. The samples were sterilized under UV light for 1 h. Then, the samples were diluted to various concentrations and added to the tested wells. After co-incubation for 1 day, the medium in the wells was aspirated, and CCK-8 reagent was added following the kit instructions. After incubation in a cell culture incubator for 1 h, the absorbance was measured at 450 nm. The cell viability rate was calculated using Equation (6):

$$\text{Cell viability rate } (\%) = \frac{(A_t - A_0)}{(A_C - A_0)} \times 100\% \quad (6)$$

A_t, A_0, and A_c represent the absorbance of the sample group, the CCK-8-only blank group, and the control group incubated for one day, respectively.

3. Results

3.1. Fabrication and Characterization of Gel/HZ@L

The preparation of Gel/HZ@L and its application in analgesia are demonstrated in Figure 1. Specifically, ZIF-8 and ZIF-8@L were synthesized using the solvothermal method, followed by coating ZIF-8 with HA through electrostatic interactions. Due to the abundance of negatively charged carboxyl groups in HA, these groups interact strongly with zinc ions, allowing HA to grow on the surface of ZIF-8, thereby forming HA-ZIF@L. Their morphology and size were observed using SEM and DLS. As shown in Figure 2, The ZIF-8 synthesized using the solvothermal method exhibited a dodecahedral structure characterized by uniform size and distinct edges and corners. After the loading of lidocaine, ZIF-8@L maintained its dodecahedral cubic structure. However, upon coating with HA, the edges and corners of the dodecahedron became less pronounced compared to their original state. The sizes of ZIF-8, ZIF-8@L, and HA-ZIF@L were 165.6 ± 2.2 nm, 178.9 ± 6.0 nm, and 233.4 ± 2.5 nm, respectively. The changes in their size and morphology demonstrated the successful encapsulation of lidocaine within ZIF-8 and the successful coating of HA onto the surface of ZIF-8.

To further explore the crystal structure of ZIF-8, ZIF@L, and HA-ZIF@L, powder X-ray diffraction (XRD) analysis was employed. As shown in Figure 3a, the diffraction pattern of ZIF-8 is in good agreement with the characteristic peaks of the previously reported ZIF-8 crystal structure simulation [14,24]. The peaks of ZIF@L are very similar to ZIF-8, indicating that the loading of lidocaine did not disrupt the crystal integrity of ZIF-8. Furthermore, no peaks characteristic to lidocaine are observed, suggesting that lidocaine was successfully incorporated as a guest molecule within the ZIF-8 crystal lattice. Nevertheless, the diffraction pattern of HA-ZIF@L exhibited partial masking, potentially attributed to the presence of a thicker HA coating on the surface of ZIF-8, providing supporting evidence for the successful cladding of HA [25].

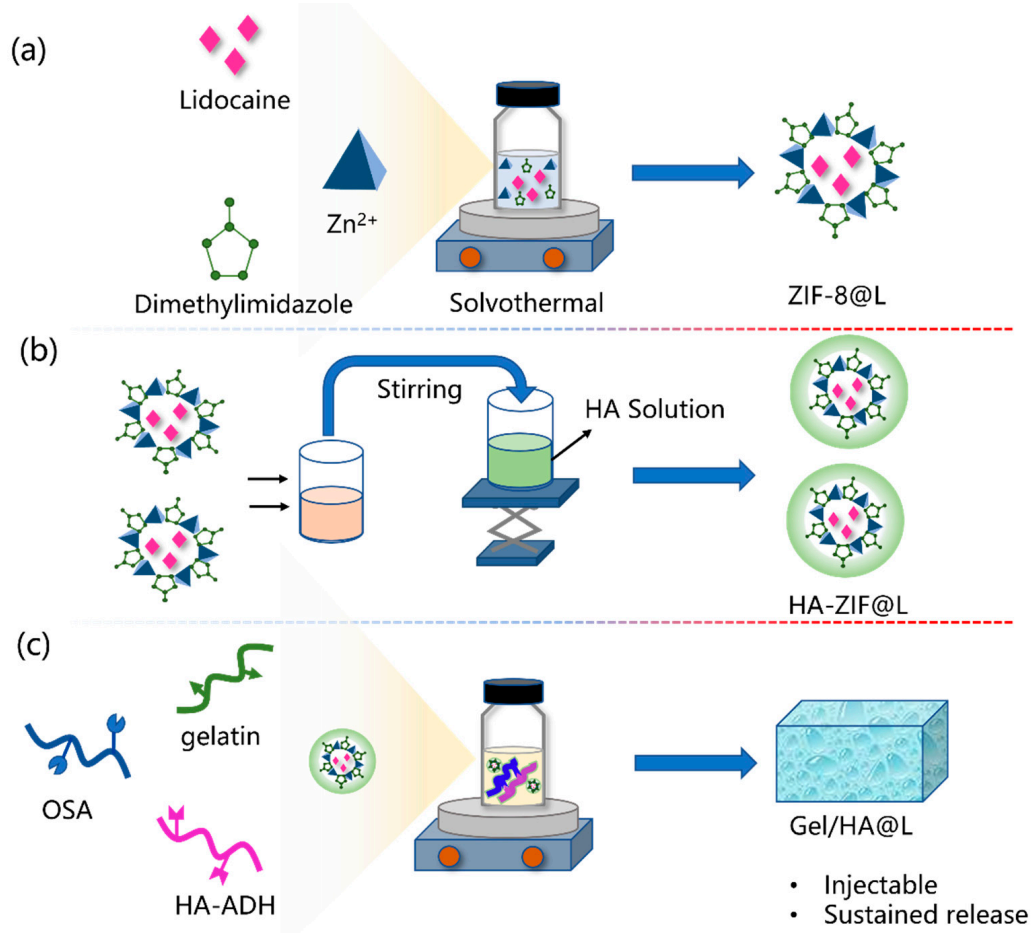

Figure 1. Schematic illustration of preparation of multi-level drug delivery system.

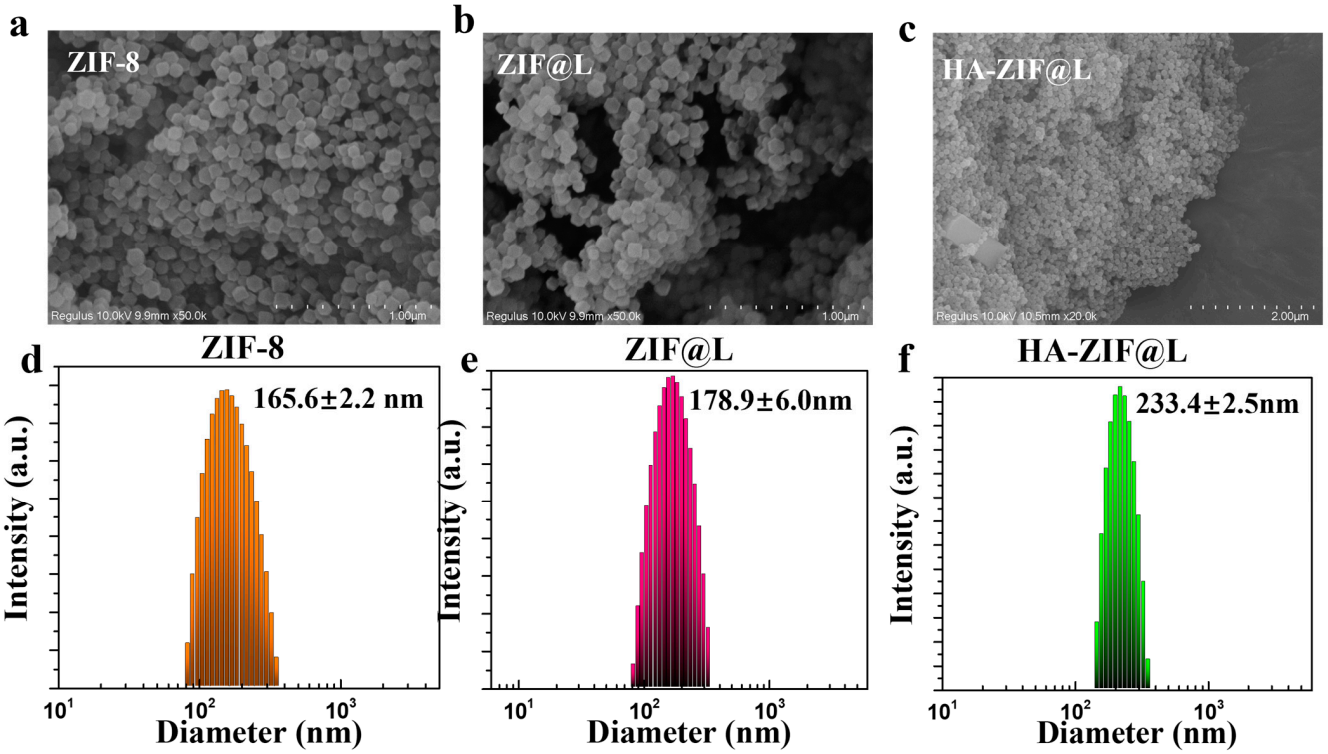

Figure 2. SEM images of (**a**) ZIF-8, (**b**) ZIF@L, and (**c**) HA-ZIF@L. Size distributions measured by DLS of (**d**) ZIF-8, (**e**) ZIF@L, and (**f**) HA-ZIF@L.

Furthermore, the structure of the lidocaine, ZIF-8, ZIF@L, and HA-ZIF@L was determined by FTIR spectrum. As shown in Figure 3b, the absorption peak at 420 cm^{-1} could be attributed to the Zn-N stretching vibration peak of ZIF-8, representing the coordination bond between Zn^{2+} and 2-methylimidazole. The peaks at 3135 cm^{-1}, 2926 cm^{-1}, and 1580 cm^{-1} correspond to the stretching vibrations of the aromatic C–H bond, aliphatic C–H bond, and C=C bond in 2-methylimidazole, respectively, are characteristic of ZIF-8.

The characteristic bands of lidocaine appear at 3250 cm^{-1} for N–H symmetric stretching and 1670 cm^{-1} for C=O stretching vibration [26]. The characteristic peak at 1670 cm^{-1} was also observed on ZIF@L, demonstrating the successful encapsulation of lidocaine. In addition, in the infrared spectrum of HA-ZIF@L, two characteristic peaks are located at 3430 cm^{-1} and 420 cm^{-1}, which could be ascribed to the O-H of hyaluronic acid and the Zn–N of ZIF-8, respectively, indicating the successful coating of HA on ZIF@L (Figure S1).

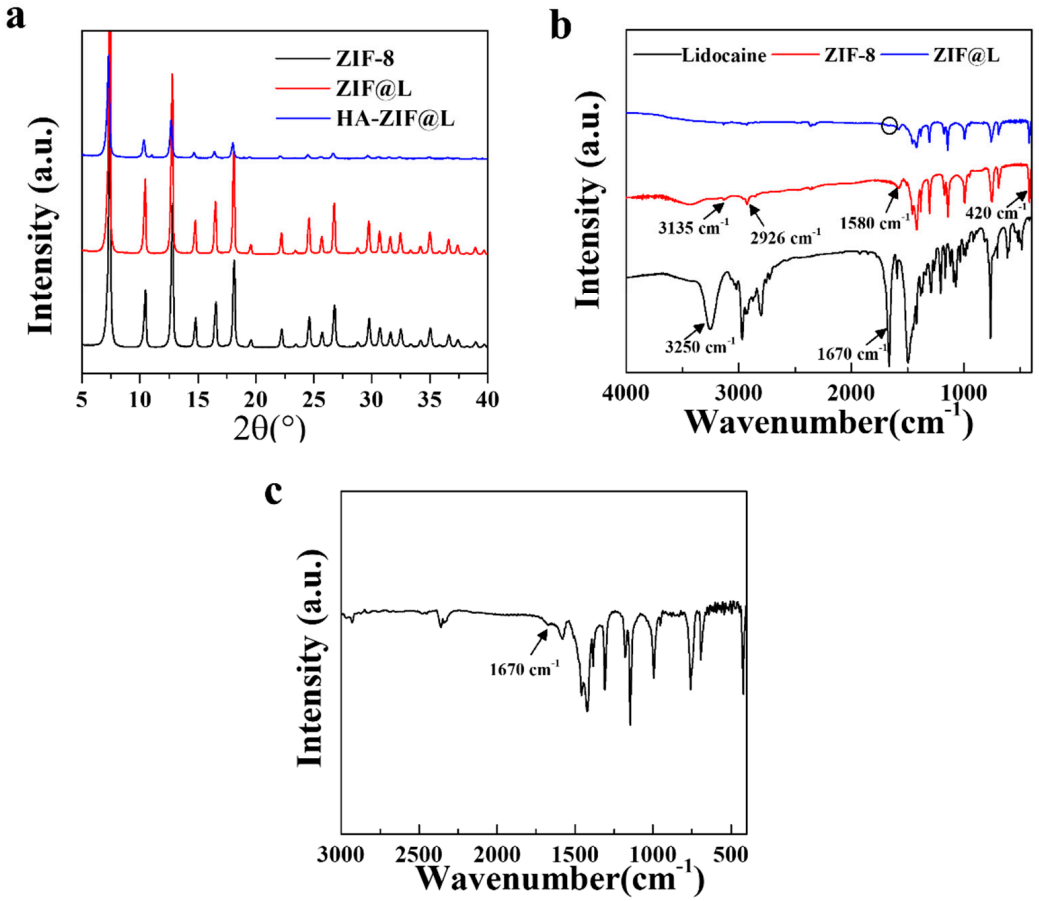

Figure 3. (**a**) XRD patterns of the as-prepared ZIF-8, ZIF-8@L, and HA-ZIF@L. (**b**) FTIR spectra of the as-prepared lidocaine, ZIF-8, and ZIF@L. (**c**) Magnification of the FTIR spectrum of ZIF@L.

To achieve sustained release of lidocaine to meet clinical needs, HA-ZIF@L was combined with injectable hydrogel to form a multi-level drug delivery system. Due to the inherent biocompatibility of natural polymers, we used them as the framework to construct injectable hydrogels. Firstly, OSA with aldehyde groups was obtained through sodium periodate oxidation, and its oxidation degree was determined to be 8 mmol/g through titration by hydroxylamine hydrochloride (Figure S2). Secondly, we grafted hydrazide groups onto hyaluronic acid via acylhydrazination. The successful grafting of the hydrazide group was verified through the nuclear magnetic resonance (NMR) spectroscopy of hydrogen. Specifically, the peak at a chemical shift of 1.8 ppm belongs to the hydrogen spectrum of the methyl group connected to the acetamide group on the hyaluronic acid molecular chain. The chemical shift between 1.8 and 2.0 ppm is attributed to the hydrogen

spectrum peak corresponding to the hydrogen on the methylene carbon in the hydrazide molecule. Through calculations, the grafting rate of the hydrazide group was determined to be 51.59% (Figure S3). Based on the above results, the multi-level drug delivery system was obtained through the one pot method by mixing OSA, HA-ADH, gelatin, and HA-ZIF@L on the vortex meter. The aldehyde groups on OSA can form reversible imine bonds with amino groups on the gelatin structure, and also reversible acylhydrazone bonds with the hydrazide bonds on HA-ADH. Meanwhile, intermolecular hydrogen bonding also contributes to the formation of hydrogel. Figure 4 shows that the hydrogels have a connected three-dimensional network structure that facilitates the transport of active molecules. Moreover, the mean pore sizes of Gel/HZ@L_0, Gel/HZ@L_1, Gel/HZ@L_2, Gel/HZ@L_3, and Gel/HZ@L_4 were 0.37 mm, 0.27 mm, 108.99 μm, 68.62 μm, and 77.36 μm, respectively. The pore size distributions of the hydrogels are shown in Figure S4. It can be observed that as the content of nanoparticles increased, the hydrogels' pore sizes decreased, likely due to the presence of nanoparticles that acted as cross-linkers, improving the degree of cross-linking of the hydrogels. In the three-dimensional network structure of Gel/HZ@L_4, the presence of HA-ZIF@L on the pore walls can be observed, demonstrating the successful synthesis of the multi-level drug delivery system combining the hydrogel and nanoparticles.

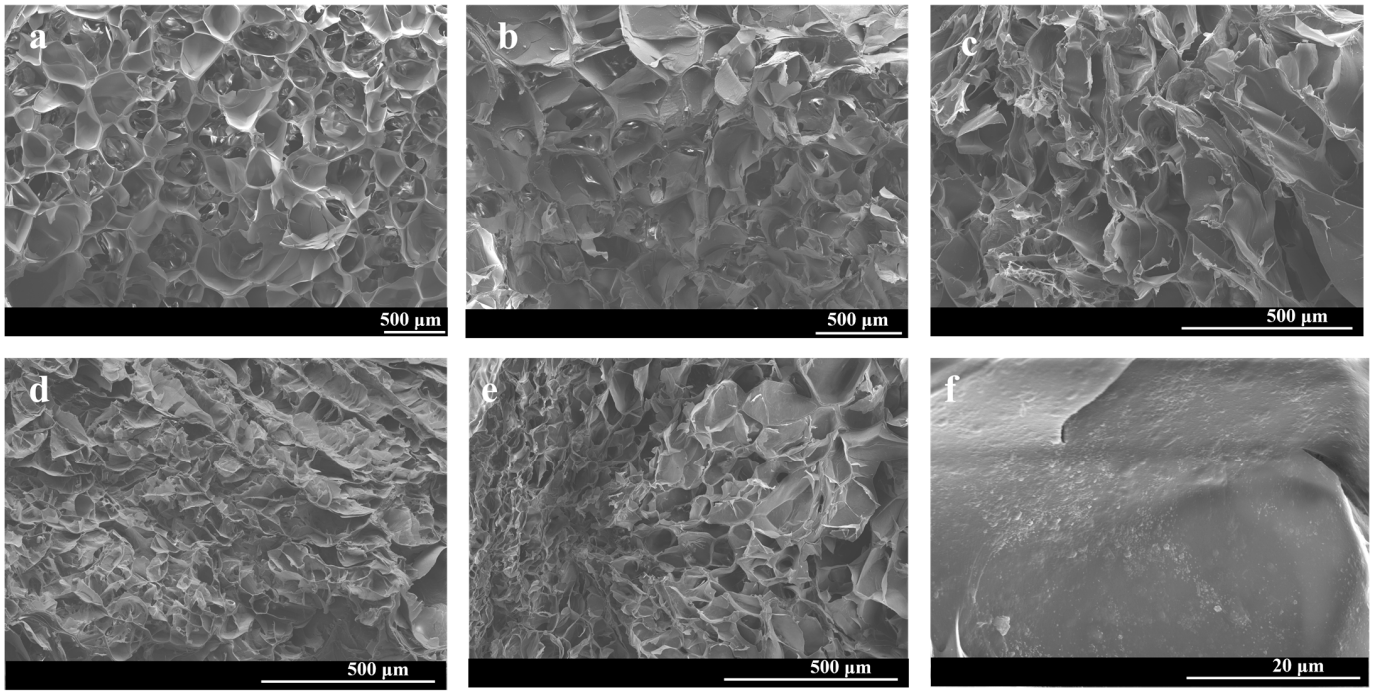

Figure 4. SEM images of (**a**) Gel/HZ@L_0, (**b**) Gel/HZ@L_1, (**c**) Gel/HZ@L_2, (**d**) Gel/HZ@L_3, (**e**) Gel/HZ@L_4, and local magnification of (**f**) Gel/HZ@L_4.

3.2. Rheological Properties of Gel/HZ@L

Furthermore, the viscoelasticity of Gel/HZ@L_0, Gel/HZ@L_1, Gel/HZ@L_2, Gel/HZ@L_3, and Gel/HZ@L_4 was characterized using a rotational rheometer. Figure 5 shows the strain sweep results of the five groups of hydrogels. The results show that the storage modulus of all experimental groups was greater than the loss modulus, and as the content of nanoparticles increased, the storage modulus also increased, from 260 Pa to 489 Pa. However, the storage modulus slightly decreased to 435 Pa with a further increase in the HA-ZIF@L content. This may be due to the increased probability of agglomeration caused by the increased content of nanoparticles. Due to the trend of hydrogel strength, Gel/HZ@L_3 was selected for subsequent studies involving injectable performance and release performance.

The injectability of the hydrogel formulation was verified through cyclic strain and shear rate scans. In Figure 5, we can see that when more than 1000% strain was applied by the rheometer, the loss modulus was less than the storage modulus, which means that the hydrogel structure was destroyed at this time. Therefore, we applied alternating strains of 1% and 2000% to the gel to observe the changes in the modulus of the hydrogel. The results are shown in Figure 6a. When 1% strain was applied, the storage modulus was greater than the loss modulus, and it was in a gel state. When 2000% strain was applied, the storage modulus was less than the loss modulus, and it was in a sol state. When the 1% strain was applied, it returned to the gel state. The results show that the reversible bond in the gel can recover autonomously.

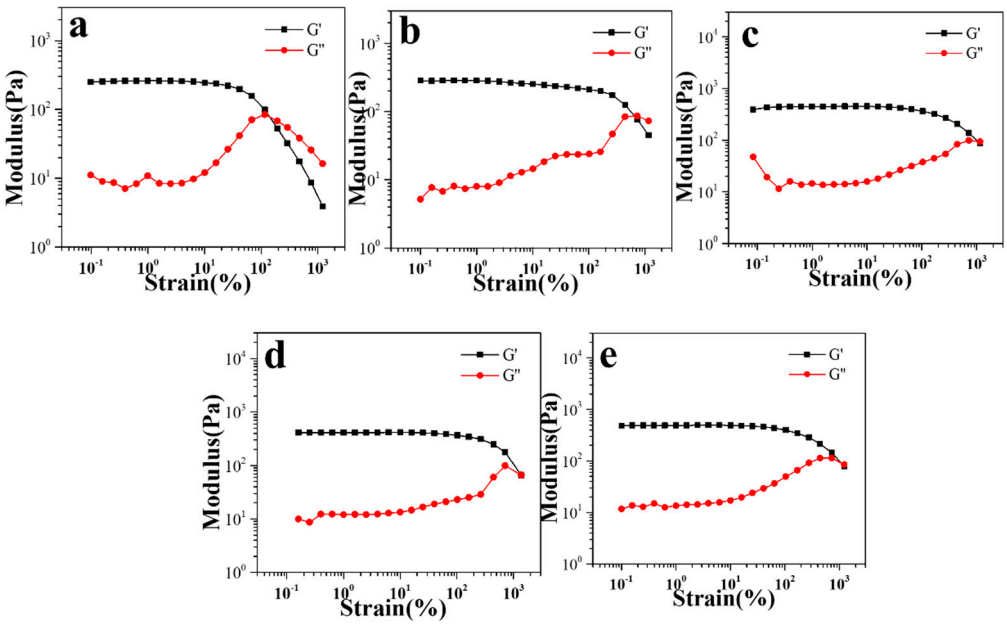

Figure 5. Strain sweep of (**a**) Gel/HZ@L_0, (**b**) Gel/HZ@L_1, (**c**) Gel/HZ@L_2, (**d**) Gel/HZ@L_3, and (**e**) Gel/HZ@L_4.

As can be seen in Figure 6b, the viscosity of the hydrogel decreased as the shear rate increased, and these properties made it injectable. The hydrogel could be extruded by 27G-needle injection (Figure 6c). We further measured the storage modulus of the gel after extrusion and found that the storage modulus was still greater than the loss modulus, and it was still in the gel state (Figure 6d). However, the modulus decreased slightly, from 485 Pa to 297 Pa, because it takes time for the reversible bond interactions to recover, and some reversible bond interactions of the newly extruded gel had not completed the recombination, resulting in a decrease in the crosslinking degree of the gel and a decrease in the modulus. The stability of the hydrogel was also evaluated, and the results show that the hydrogel was stable and could maintain a gel state after soaking in PBS for 3 days (Figure 6e).

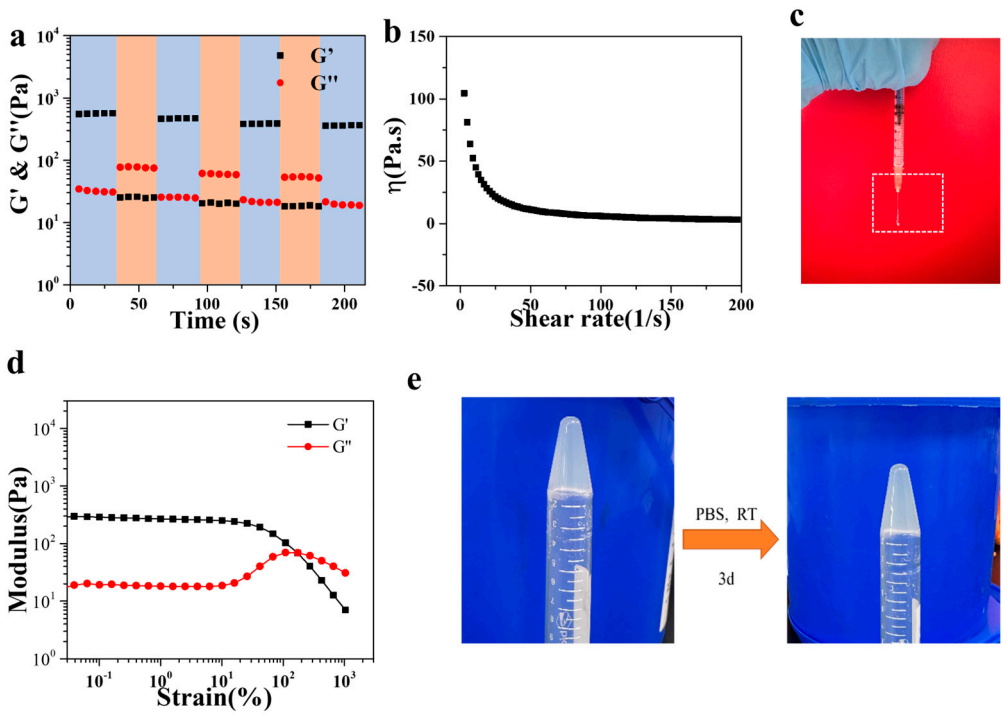

Figure 6. (**a**) The storage modulus and loss modulus of Gel/HZ@L_3 under repeated deformation at 1% and 2000% (high) strain at 10 Hz. (**b**) The viscosity of Gel/HZ@L_3 as a function of the shear rate. (**c**) A photograph of the Gel/HZ@L_3 squeezed out through a 27G syringe. (**d**) The modulus of Gel/HZ@L_3 after extrusion. (**e**) A photograph of the gel after three days of soaking in PBS solution.

3.3. Release Behavior of HZ@L and Gel/HZ@L

Finally, the release behavior of lidocaine embedded in HA-ZIF and the multi-level release system were investigated. The encapsulation efficiency of lidocaine loaded into the nanoparticles was calculated to be 35.7%. As depicted in Figure 7, under pH 7.4 conditions, HA-ZIF@L and Gel/HZ@L_3 exhibited extremely low drug release rates, at 9.8% and 5.9% respectively, because of the high stability of ZIF-8 and the hydrogel network. However, under acidic conditions with a pH of 5.4, the drug release rates in HA-ZIF@L and Gel/HZ@L_3 reached 83.7% and 67.9%, respectively. This phenomenon can be attributed to the protonation of the 2-methylimidazole, which leads to the disruption of the coordination bond between the zinc ion and the imidazole acid ring in ZIF-8. Consequently, this enabled the release of the lidocaine that was embedded within the cavity structure of ZIF-8. Additionally, Schiff base bonds decompose under acidic conditions, resulting in the collapse of the hydrogel network and the release of drug molecules. Therefore, in acidic conditions, the release rate of lidocaine in the multi-level drug release system was significantly faster compared to that under neutral conditions. However, compared to the single HA-ZIF drug delivery system, the multi-level release system integrating hydrogel and HA-ZIF exhibited significant sustained release properties, and it could be continuously released for more than 96 h, meeting the clinical needs of postoperative analgesia and indicating its potential application in the field of long-acting sustained-release formulations. It should be noted that this work represents a conceptual and foundational investigation into the development of a nanoparticle/gel-based formulation for subcutaneous injection, aimed at achieving sustained analgesic delivery. While the design, formulation, and preliminary characterization demonstrate promising potential for long-acting pain management, this study is exploratory in nature. Critical parameters, including optimal dosing and pharmacokinetics, have not yet been fully established. Further preclinical and clinical studies are required to validate the efficacy and determine appropriate dosage regimens. This foundational

research serves as a critical step toward advancing the development of innovative analgesic delivery systems, but additional work is necessary to translate these findings into practical therapeutic applications.

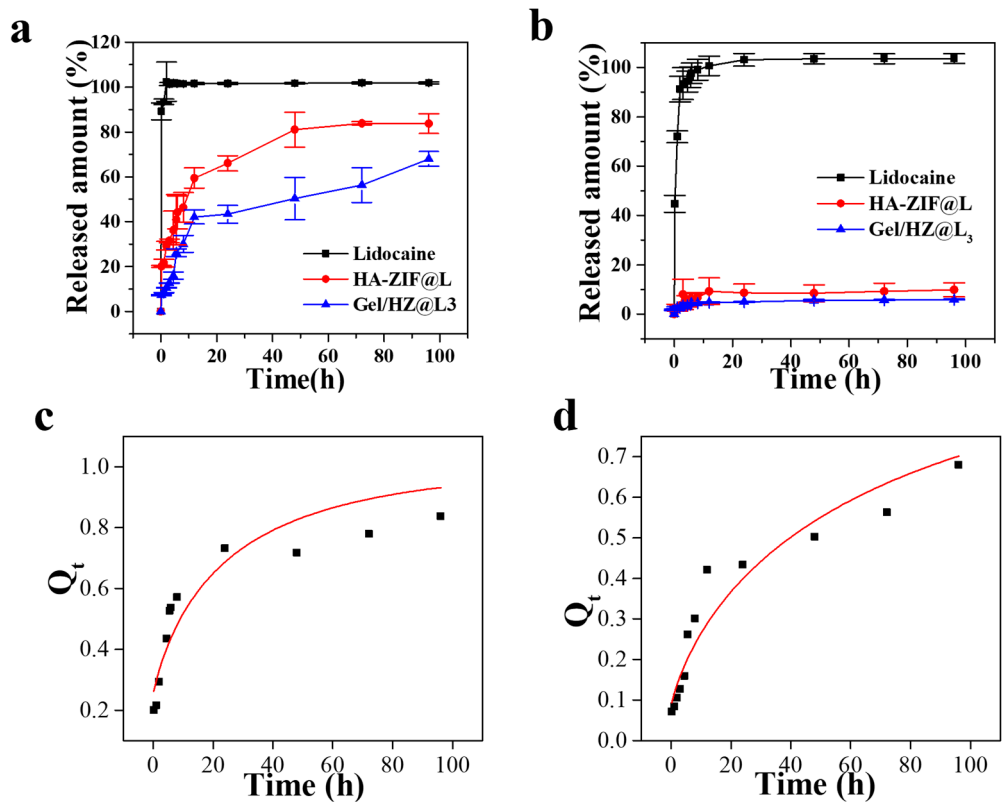

Figure 7. In vitro release of lidocaine from HA-ZIF@L and Gel/HZ@L_3 in PBS at (**a**) pH 5.4 and (**b**) pH 7.4. Release data of lidocaine from (**c**) HA-ZIF@L and (**d**) Gel/HZ@L_3 in PBS pH 5.4 conditions, fitted with Bshakar models.

3.4. Lidocaine Release Mechanism

The release mechanism refers to the release mode of an interior ingredient from the carrier, usually including diffusion, dissolution, swelling, degradation, and erosion [27,28]. The resulting release mechanism is determined by the matrix system in nature, external conditions, and so on. From the fitting results in Table S2, it can be seen that the lidocaine release from HA-ZIF@L under acidic conditions is more in line with the Bhaskar model, with an R2 of 0.8335. The Gel/HZ@L_3 drug release curves were fitted by the Higuchi model and the Bhaskar model with correlation coefficients of 0.9133 and 0.9127, respectively, which confirm that both models could be used to describe the release kinetics of lidocaine. Therefore, the release mechanism of lidocaine in the HA-ZIF@L and Gel/HZ@L_3 systems can be attributed to the dissolution and ion exchange process of ZIF-8 [29,30]. This process entailed a diffusion control mechanism of lidocaine involving outer surface diffusion through ion exchange and intraparticulate diffusion. In the initial stage of release, a portion of the lidocaine was adsorbed on the surface of HA-ZIF@L, with the lidocaine base on the surface exhibiting greater ease of diffusion into PBS through ion exchange. On the other hand, lidocaine trapped within the HA-ZIF@L particles diffused from the inside toward the surface, resulting a longer diffusion time to reach the PBS solution. Given the increased instability of ZIF-8 under acidic conditions, along with the increased intensity of the ion exchange process, the release of lidocaine in ZIF-8 occurred at a faster rate compared to neutral conditions. It is worth noting that we also simulated the release behavior of

HA-ZIF@L and Gel/HZ@L_3 under acidic conditions with the Korsmeyer–Peppas model, and the fitting correlation coefficients were 0.8302 and 0.9042, respectively.

3.5. Cytotoxicity and Biocompatibility

A Cck-8 kit was applied to assess the biocompatibility of HA-ZIF@L on normal fibroblast (L929) cells, which is displayed in Figure 8. Compared with a positive control group (DMEM+10%DMSO), the HA-ZIF@L groups exhibit excellent biocompatibility. After 24 h of incubation, over 85% cells treated with HA-ZIF@L at the highest concentration (120 μg/mL) were alive. Meanwhile, the cells treated with HA-ZIF@L at 90 μg/mL, 60 μg/mL, and 30 μg/mL showed 97.3%, 88.4%, and 103.3% viability, respectively.

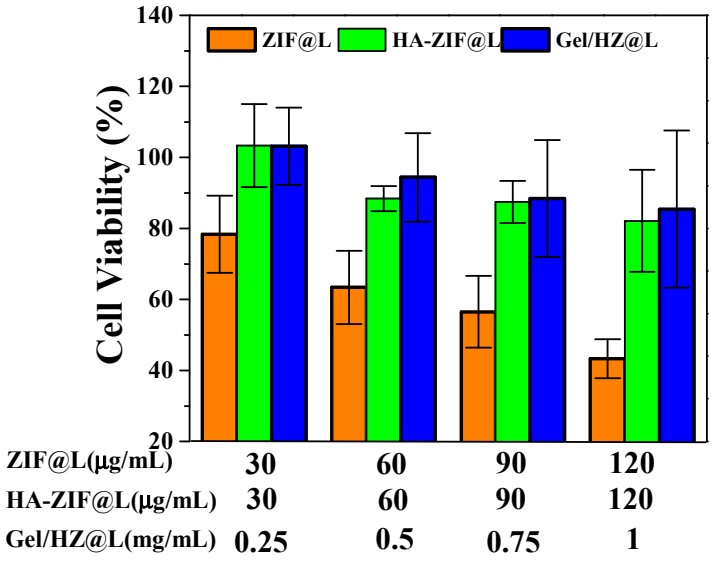

Figure 8. In vitro cytotoxicity of L929 cells incubated with different samples at various concentrations for 24 h.

4. Discussion

In this work, in the above investigation, a multi-level drug loading system based on nanoparticles/injectable hydrogels was constructed to delay the release rate of lidocaine. First, lidocaine was loaded into ZIF-8 nanoparticles, and the ZIF-8 was further coated with hyaluronic acid to enhance its dispersion and improve its biocompatibility. The morphology and particle size changes of the nanoparticles before and after drug loading were observed by SEM and DLS. Similarly, the morphology and particle size of the nanoparticles after being coated with hyaluronic acid were evaluated by the same methods. It was found that the size of the nanoparticles increased after the drug loading and hyaluronic acid coating, which proves the successful loading of lidocaine and successful coating of hyaluronic acid. The structural changes of the nanoparticles were further verified by XRD and FTIR. According to the results of the pattern, the structure of ZIF-8 was not changed by the loading of lidocaine, and the coating of hyaluronic acid showed partial masking, which may be due to the existence of a thick HA coating on the surface of ZIF-8, providing supporting evidence for the successful coating of HA. This is consistent with the findings of Lin et al. [31]. The characteristic peaks of ZIF-8 and lidocaine can be observed in the FTIR spectra of ZIF@L, which further prove the successful loading of lidocaine.

After the successful preparation of HA-ZIF@L, we constructed injectable hydrogels through the Schiff base reaction and combined the nanoparticles with the injectable hydrogels to construct a multi-level drug loading system, which could further delay the release of lidocaine. Injectable hydrogels were prepared using hydrazideated hyaluronic acid, oxidized sodium alginate, and gelatin through reversible bonding. Injectable hydrogels have

higher viscosity and can extend the drug retention time to achieve slow release compared to other carriers. In order to study the effects of nanoparticle combination on injectable hydrogels, we constructed injectable hydrogels with different nanoparticle contents. The microscopic morphology of the hydrogels was observed by SEM. The results show that the increase in nanoparticle content would lead to an increase in the crosslinking density, which would lead to a tighter network. The rheology results are consistent with those observed in the morphology. However, further increasing the nanoparticle content led to a slight decrease in the modulus, possibly due to the aggregation of nanoparticles. Injectable hydrogel has shear-thinning properties, allowing it to be extruded through a 27 G needle. This provides convenience for its subsequent practical use.

In order to verify the advantage of a multi-level drug loading system, the drug release behaviors of HA-ZIF@L and Gel/HZ@L were tested, and the results show that the multi-level drug loading hydrogels could further delay drug release. Chen et al. found that multi-level systems, such as microspheres/gels and fibers/gels, can also significantly delay drug release [19]. In addition, Gel/HZ@L has good biocompatibility, and HA-ZIF@L, with the same concentration, has better biocompatibility than ZIF@L, indicating that the coating of HA has the effect of improving the biocompatibility of nanoparticles.

5. Conclusions

In summary, our study has demonstrated that Gel/HZ could be a very promising system for the sustained release of lidocaine for pain relief. A facile yet versatile procedure has been proposed for encapsulating lidocaine into ZIF-8, followed by coating with an HA shell. The resulting HZ@L particles were uniformly dispersed within a hydrogel crosslinked by Schiff base bonds. The Gel/HZ hydrogel containing lidocaine exhibited cytocompatibility, injectability, and sustained release for over 96 h. Furthermore, the Gel/HZ hydrogel system resulted in a moderate reduction in burst release compared to the HA/ZIF-8 nano-system. This multi-level drug delivery system integrating nanoparticles and hydrogel has the potential to reduce opioid consumption and provide localized, sustained release of analgesics. In the future, the use of this hydrogel formulation can be extended to other encapsulated drugs.

Supplementary Materials: The following supporting information can be downloaded at: https://www.mdpi.com/article/10.3390/jpbi2010003/s1, Figure S1: FTIR spectra of as-prepared HA-ZIF@L. Figure S2: NMR spectra of HA-ADH. Figure S3: Hydroxylamine hydrochloride-potential titration curve of sodium alginate oxide. Figure S4: Statistical histogram of the pore size of Gel/HZ@L_0, Gel/HZ@L_1, Gel/HZ@L_2, Gel/HZ@L_3, Gel/HZ@L_4. Table S1: Composition of Gel/HZ@L hydrogels. Table S2: Fitting results of lidocaine release kinetics parameters using different models at pH 5.4 and pH 7.4.

Author Contributions: Conceptualization, L.J.; methodology, L.J. and X.W.; validation, J.Z. and F.Z.; formal analysis, L.J.; investigation, L.J.; resources, L.J.; data curation, L.J. and X.W.; writing—original draft preparation, L.J.; writing—review and editing, S.A. and F.F.; visualization, L.J.; supervision, J.Z. and S.A.; project administration, J.Z., F.Z. and L.J.; funding acquisition, L.J. All authors have read and agreed to the published version of the manuscript.

Funding: This work was supported by the Natural Science Foundation of Ningbo (Grant No. 2023J370) and China Postdoctoral Science Foundation (Grant No. 2023M733599), with Lei Jiang as the recipient. The authors are thankful for the financial support from NIMTE, CAS.

Institutional Review Board Statement: Not applicable.

Informed Consent Statement: Not applicable.

Data Availability Statement: The raw data supporting the conclusions of this article will be made available by the authors upon request.

Acknowledgments: The authors thank Junhui Yang for her assistance in the XRD analyses.

Conflicts of Interest: Shaukat Ali is an employee of Ascendia Pharma, Inc., USA. The other authors declare no conflicts of interest.

References

1. Peng, F.; Liu, J.; Chen, J.; Wu, W.; Zhang, Y.; Zhao, G.; Kang, Y.; Gong, D.; He, L.; Wang, J.; et al. Nanocrystals Slow-Releasing Ropivacaine and Doxorubicin to Synergistically Suppress Tumor Recurrence and Relieve Postoperative Pain. *ACS Nano* **2023**, *17*, 20135–20152. [CrossRef] [PubMed]
2. He, Y.; Qin, L.; Fang, Y.; Dan, Z.; Shen, Y.; Tan, G.; Huang, Y.; Ma, C. Electrospun PLGA nanomembrane: A novel formulation of extended-release bupivacaine delivery reducing postoperative pain. *Mater. Des.* **2020**, *193*, 108768. [CrossRef]
3. Brigham, N.C.; Ji, R.-R.; Becker, M.L. Degradable polymeric vehicles for postoperative pain management. *Nat. Commun.* **2021**, *12*, 1367. [CrossRef]
4. Wang, H.; Zhang, Y.; Xu, X.; Wang, A. An injectable mesoporous silica-based analgesic delivery system prolongs the duration of sciatic nerve block in mice with minimal toxicity. *Acta Biomater.* **2021**, *135*, 638–649. [CrossRef]
5. Callahan, G.; Veith, A.; Madariaga, A.; Rausch, M.K.; Stromberg, D.; Baker, A.B. Drug eluting chest tube with sustained release of local anesthetic agents for pain reduction. *Appl. Mater. Today* **2023**, *32*, 101817. [CrossRef]
6. Peng, F.; Liu, J.; Zhang, Y.; Fan, J.; Gong, D.; He, L.; Zhang, W.; Qiu, F. Designer self-assembling peptide nanofibers induce biomineralization of lidocaine for slow-release and prolonged analgesia. *Acta Biomater.* **2022**, *146*, 66–79. [CrossRef] [PubMed]
7. Steverink, J.G.; van Tol, F.R.; Oosterman, B.J.; Vermonden, T.; Verlaan, J.-J.; Malda, J.; Piluso, S. Robust gelatin hydrogels for local sustained release of bupivacaine following spinal surgery. *Acta Biomater.* **2022**, *146*, 145–158. [CrossRef]
8. Wang, P.; Wang, G.; Tang, H.; Feng, S.; Tan, L.; Zhang, P.; Wei, G.; Wang, C. Preparation of Ropivacaine Encapsulated by Zeolite Imidazole Framework Microspheres as Sustained-Release System and Efficacy Evaluation. *Chem. Eur. J.* **2023**, *29*, e202203458. [CrossRef]
9. Blair, H.A. Bupivacaine/Meloxicam Prolonged Release: A Review in Postoperative Pain. *Drugs* **2021**, *81*, 1203–1211. [CrossRef] [PubMed]
10. Yuan, X.; Liu, X.; Li, H.; Peng, S.; Huang, H.; Yu, Z.; Chen, L.; Liu, X.; Bai, J. pH-Triggered Transformable Peptide Nanocarriers Extend Drug Retention for Breast Cancer Combination Therapy. *Adv. Healthc. Mater.* **2024**, 2400031. [CrossRef] [PubMed]
11. Yang, H.; Wang, S.; Bian, H.; Xing, X.; Yu, J.; Wu, X.; Zhang, L.; Liang, X.; Lu, A.; Huang, C. Extracellular matrix-mimicking nanofibrous chitosan microspheres as cell micro-ark for tissue engineering. *Carbohyd. Polym.* **2022**, *292*, 119693. [CrossRef]
12. Khalili, Z.; Kazemi, N.M.; Azar, Z.J.; Mosavi, Z.; Hasanzadeh, M. Fabrication and characterization of a Bi2O3-modified chitosan@ZIF-8 nanocomposite for enhanced drug loading-releasing efficacy. *Int. J. Biol. Macromol.* **2024**, *263*, 130295. [CrossRef]
13. Zhang, X.; Chen, J.; Pei, X.; Yang, L.; Wang, L.; Chen, L.; Yang, G.; Pei, X.; Wan, Q.; Wang, J. Drug-loading ZIF-8 for modification of microporous bone scaffold to promote vascularized bone regeneration. *Chin. Chem. Lett.* **2024**, *35*, 108889. [CrossRef]
14. Wang, B.; Zhang, S.; Shen, Z.-T.; Hou, T.; Zhao, Y.-H.; Huang, M.-S.; Li, J.; Chen, H.; Hu, P.-H.; Luo, Z.-J.; et al. Core-Shell Reactor Partitioning Enzyme and Prodrug by ZIF-8 for NADPH-Sensitive In Situ Prodrug Activation. *Angew. Chem. Int. Edit.* **2023**, *62*, e202314025. [CrossRef] [PubMed]
15. Lee, Y.-M.; Lu, Z.-W.; Wu, Y.-C.; Liao, Y.-J.; Kuo, C.-Y. An injectable, chitosan-based hydrogel prepared by Schiff base reaction for anti-bacterial and sustained release applications. *Int. J. Biol. Macromol.* **2024**, *269*, 131808. [CrossRef] [PubMed]
16. Cao, Z.; Chen, Y.; Bai, S.; Zheng, Z.; Liu, Y.; Gui, S.; Shan, S.; Wu, J.; He, N. In situ formation of injectable organogels for punctal occlusion and sustained release of therapeutics: Design, preparation, in vitro and in vivo evaluation. *Int. J. Pharmaceut.* **2023**, *638*, 122933. [CrossRef]
17. Fahmy-Garcia, S.; Mumcuoglu, D.; de Miguel, L.; Dieleman, V.; Witte-Bouma, J.; van der Eerden, B.C.J.; van Driel, M.; Eglin, D.; Verhaar, J.A.N.; Kluijtmans, S.G.J.M.; et al. Novel In Situ Gelling Hydrogels Loaded with Recombinant Collagen Peptide Microspheres as a Slow-Release System Induce Ectopic Bone Formation. *Adv. Healthc. Mater.* **2018**, *7*, 1800507. [CrossRef] [PubMed]
18. Jimenez, J.; Resnick, J.L.; Chaudhry, A.B.; Gertsman, I.; Nischal, K.K.; DiLeo, M.V. Ocular biodistribution of cysteamine delivered by a sustained release microsphere/thermoresponsive gel eyedrop. *Int. J. Pharmaceut.* **2022**, *624*, 121992. [CrossRef] [PubMed]
19. Zhang, W.; Ning, C.; Xu, W.; Hu, H.; Li, M.; Zhao, G.; Ding, J.; Chen, X. Precision-guided long-acting analgesia by Gel-immobilized bupivacaine-loaded microsphere. *Theranostics* **2018**, *8*, 3331–3347. [CrossRef]
20. Zhang, W.; Xu, W.; Ning, C.; Li, M.; Zhao, G.; Jiang, W.; Ding, J.; Chen, X. Long-acting hydrogel/microsphere composite sequentially releases dexmedetomidine and bupivacaine for prolonged synergistic analgesia. *Biomaterials* **2018**, *181*, 378–391. [CrossRef] [PubMed]

21. Zhuang, J.; Kuo, C.-H.; Chou, L.-Y.; Liu, D.-Y.; Weerapana, E.; Tsung, C.-K. Optimized Metal–Organic-Framework Nanospheres for Drug Delivery: Evaluation of Small-Molecule Encapsulation. *ACS Nano* **2014**, *8*, 2812–2819. [CrossRef] [PubMed]
22. Zhao, L.; Feng, Z.; Lyu, Y.; Yang, J.; Lin, L.; Bai, H.; Li, Y.; Feng, Y.; Chen, Y. Electroactive injectable hydrogel based on oxidized sodium alginate and carboxymethyl chitosan for wound healing. *Int. J. Biol. Macromol.* **2023**, *230*, 123231. [CrossRef] [PubMed]
23. Yang, B.; Song, J.; Jiang, Y.; Li, M.; Wei, J.; Qin, J.; Peng, W.; Lasaosa, F.L.; He, Y.; Mao, H.; et al. Injectable Adhesive Self-Healing Multicross-Linked Double-Network Hydrogel Facilitates Full-Thickness Skin Wound Healing. *ACS Appl. Mater. Interfaces* **2020**, *12*, 57782–57797. [CrossRef]
24. Hsieh, C.-T.; Ariga, K.; Shrestha, L.K.; Hsu, S.-H. Development of MOF Reinforcement for Structural Stability and Toughness Enhancement of Biodegradable Bioinks. *Biomacromolecules* **2021**, *22*, 1053–1064. [CrossRef]
25. Sun, Q.; Bi, H.; Wang, Z.; Li, C.; Wang, X.; Xu, J.; Zhu, H.; Zhao, R.; He, F.; Gai, S.; et al. Hyaluronic acid-targeted and pH-responsive drug delivery system based on metal-organic frameworks for efficient antitumor therapy. *Biomaterials* **2019**, *223*, 119473. [CrossRef]
26. Bakhtiari, S.E.; Zhu, Z.; Magdysyuk, O.V.; Brocchini, S.; Williams, G.R. Amorphous solid dispersions of lidocaine and lidocaine HCl produced by ball milling with well-defined RAFT-synthesised methacrylic acid polymers. *Int. J. Pharmaceut.* **2023**, *644*, 123291. [CrossRef] [PubMed]
27. Xiao, Y.; Huang, Q.; Zheng, Z.; Ma, H. Selenium release kinetics and mechanism from Cordyceps sinensis exopolysaccharide-selenium composite nanoparticles in simulated gastrointestinal conditions. *Food Chem.* **2021**, *350*, 129223. [CrossRef] [PubMed]
28. Dao, L.; Chen, S.; Sun, X.; Pang, W.; Zhang, H.; Liao, J.; Yan, J.; Pang, J. Construction and sustained release of konjac glucomannan/naringin composite gel spheres. *Front. Nutr.* **2023**, *9*, 1123494. [CrossRef]
29. Cai, W.; Zhang, W.; Chen, Z. Magnetic Fe_3O_4@ZIF-8 nanoparticles as a drug release vehicle: pH-sensitive release of norfloxacin and its antibacterial activity. *Colloid Surf. B* **2023**, *223*, 113170. [CrossRef] [PubMed]
30. Li, Y.; Bi, H.-Y.; Li, H.; Mao, X.-M.; Liang, Y.-Q. Synthesis; characterization, and sustained release property of Fe3O4@(enrofloxacin-layered double hydroxides) nanocomposite. *Mat. Sci. Eng C-Mater.* **2017**, *78*, 886–891. [CrossRef] [PubMed]
31. Duan, S.; Zhao, X.; Su, Z.; Wang, C.; Lin, Y. Layer-by-Layer Decorated Nanoscale ZIF-8 with High Curcumin Loading Effectively Inactivates Gram-Negative and Gram-Positive Bacteria. *ACS Appl. Bio Mater.* **2020**, *3*, 3673–3680. [CrossRef]